

SUPPLEMENTARY INFORMATION

Myocardial Pyruvate Metabolism Before and After CABG in Three-Vessel Disease Using Hyperpolarized Carbon-13 MRI

Gaurav Sharma, PhD, MBA^{a,b,c,#}, Jaidip M. Jagtap, PhD^d, Sung-Han Lin, PhD^b, Jae Mo Park, PhD^{b,c,e,f}, Crystal E. Harrison, PhD^b, Jennine Leary, RN^b, Sarah S. McNeil, RN^a, Corey Mozingo, BS^b, Craig R. Malloy, MD^{b,e,f,g,h}, Matthias Peltz, MD^a, Michael E. Jessen, MD^{a,#}

From the ^aDepartment of Cardiovascular and Thoracic Surgery, The University of Texas Southwestern Medical Center, Dallas, TX, USA; ^bAdvanced Imaging Research Center, The University of Texas Southwestern Medical Center, Dallas, TX, USA; ^cDepartment of Biomedical Engineering, The University of Texas Southwestern Medical Center, Dallas, TX, USA; ^dRadiology, Mayo Clinic, Rochester, Minnesota, USA; ^eDepartment of Radiology, The University of Texas Southwestern Medical Center, Dallas, TX, USA; ^fCharles and Jane Pak Center for Mineral Metabolism and Clinical Research, The University of Texas Southwestern Medical Center, Dallas, TX, USA; ^gDepartment of Internal Medicine, The University of Texas Southwestern Medical Center, Dallas, TX, USA; ^hVA North Texas Healthcare System, Dallas, TX, USA

#ADDRESS FOR CORRESPONDENCE (Joint Correspondence):

Gaurav Sharma, PhD, MBA
Assistant Professor
Cardiovascular and Thoracic Surgery
UT Southwestern Medical Center
5323 Harry Hines Blvd, Dallas, TX 75390,
United States
Email: gaurav.sharma@utsouthwestern.edu

Michael E. Jessen, MD
Professor and Chairman
Cardiovascular and Thoracic Surgery
UT Southwestern Medical Center
5323 Harry Hines Blvd, Dallas, TX 75390,
United States
Email: michael.jessen@utsouthwestern.edu

CONTENTS

Supplementary Table 1. Baseline Laboratory Parameters

Supplementary Table 2. Clinical Course of the CAD patients

Supplementary Figure 1. Study Workflow and Quality Control Process

Supplementary Figure 2. Metabolism and HP-¹³CMRAnalyst Software Interface

Supplementary Figure 3. Reproducibility Assessment

Supplementary Figure 4. Pyruvate metabolism in Healthy vs Pre-CABG subjects

Supplementary Figure 5. Lactate/THCP Ratio Maps in Healthy vs Pre-CABG subjects

Supplementary Figure 6. Lactate/THCP Ratio Maps in Pre-CABG vs Post-CABG

Supplementary Figure 7. Anatomical Overlay of Metabolite Maps in Healthy vs Pre-CABG

Supplementary Figure 8. Apparent k_{PB} Rate Constant Maps

Supplementary Figure 9. Apparent k_{PL} Rate Constant Maps

Supplementary Figure 10. k_{PL} Rate Constant Polar Maps

Supplementary Materials and Methods. Enrollment Criteria, Postoperative Metabolic Changes and Clinical Course of CAD subjects, Detailed Kinetic Analysis Protocol

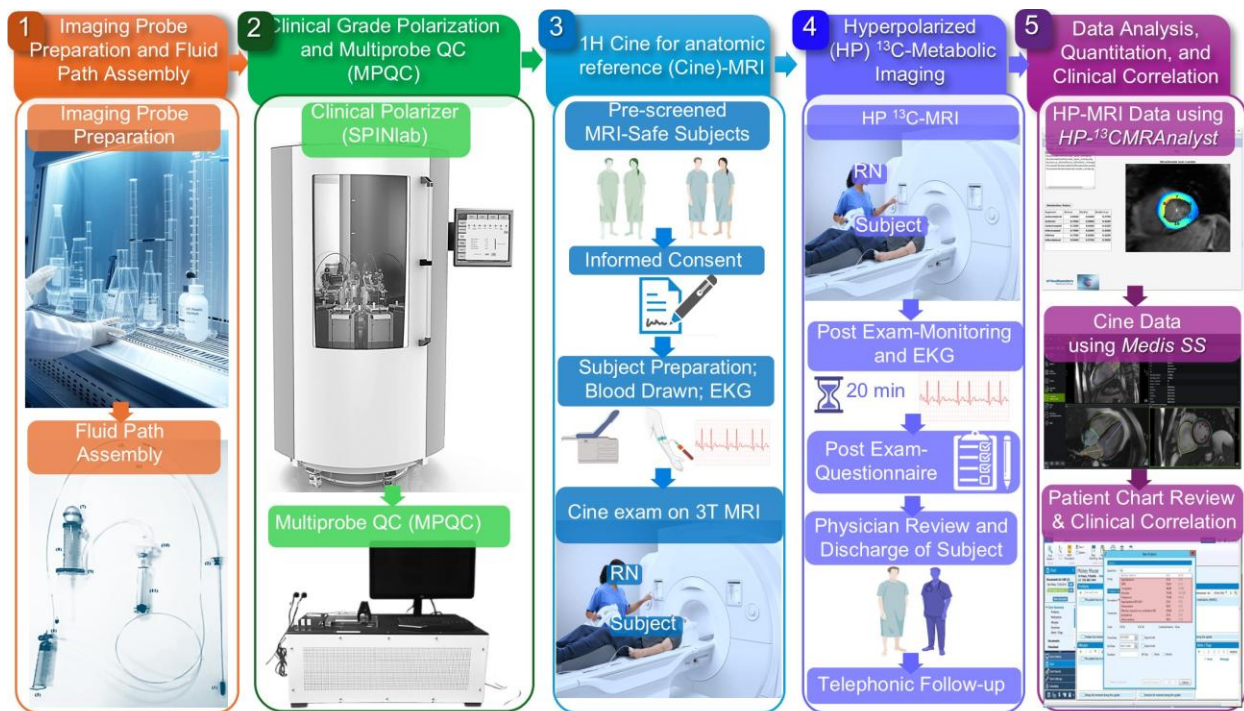
Laboratory Parameter	Mean \pm SD	Range	Reference Range*
Renal Function & Electrolytes			
Sodium, mmol/L	140.2 \pm 3.6	137 – 144	135 – 145
Potassium, mmol/L	4.1 \pm 0.3	3.7 – 4.5	3.6 – 5.0
Chloride, mmol/L	107.2 \pm 1.6	105 – 109	98 – 109
Bicarbonate (CO ₂), mmol/L	25.0 \pm 2.7	22 – 29	22 – 31
BUN, mg/dL	12.6 \pm 2.7	8 – 15	6 – 23
Creatinine, mg/dL	0.92 \pm 0.19	0.69 – 1.11	0.72 – 1.25
eGFR, mL/min/1.73m ²	89.4 \pm 15.1	76 – 114	\geq 60
Metabolic & Liver Panel			
Glucose, mg/dL	94.6 \pm 13.3	81 – 110	70 – 139
Hemoglobin A1c, %	5.6 \pm 0.3	5.3 – 6.0	4.3 – 5.6
Albumin, g/dL	4.4 \pm 0.2	4.1 – 4.7	3.5 – 5.2
Total Bilirubin, mg/dL	0.68 \pm 0.22	0.4 – 1.0	0.2 – 1.3
ALT, U/L	57.8 \pm 54.2	22 – 153	10 – 50
AST, U/L	36.2 \pm 18.6	23 – 68	10 – 50
Hematology & Coagulation			
WBC Count, $\times 10^9/L$	6.21 \pm 2.19	3.72 – 9.56	4.00 – 11.00
Hematocrit, %	44.1 \pm 4.5	36.6 – 47.7	37.0 – 50.0
INR	1.02 \pm 0.04	1.0 – 1.1	0.9 – 1.3

Supplementary Table 1: Baseline Laboratory Parameters in CAD Patients Pre-CABG. Values are mean \pm SD. ALT = alanine aminotransferase; AST = aspartate

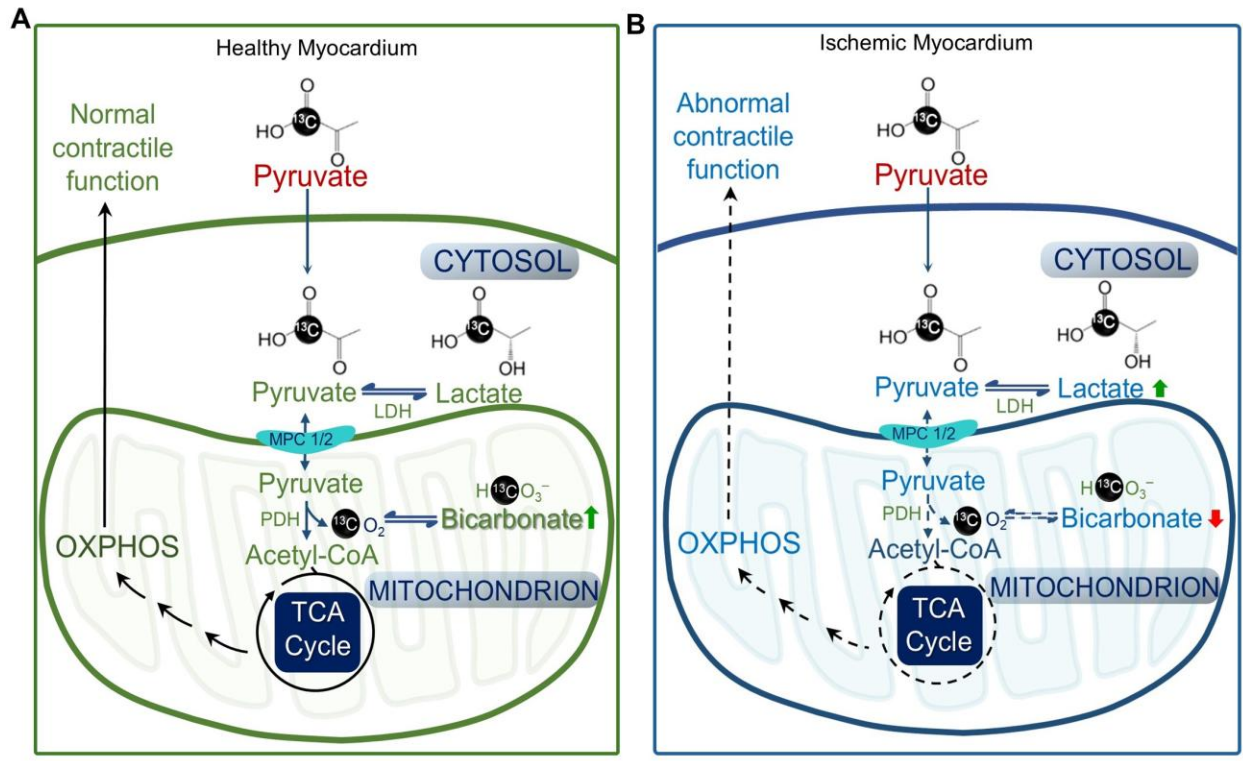
aminotransferase; BUN = blood urea nitrogen; eGFR = estimated glomerular filtration rate; INR = international normalized ratio; WBC = white blood cell.

Patient ID (Age/Sex)	Coronary Anatomy	Left Ventricular Ejection Fraction (LVEF)		Surgical Revascularization
		Pre-CABG	Post-CABG	Grafts & Targets
CAD1 (60y/ M)	3-Vessel Disease • 90% proximal LAD • 99% proximal LCx • 90% proximal R-PDA	61.0	50.5	CABG x 3 • LIMA → LAD • RIMA → PDA • SVG → Ramus
CAD 2 (78y/M)	3-Vessel Disease • 90% mid-LAD • 100% LCx • 100% RCA	32.4	30.5	CABG x 3 • LIMA → LAD • SVG → OM • SVG → PDA
CAD3 (60y/M)	Severe 3-Vessel Disease • 95% proximal LAD • 90% Ramus • 100% distal RCA	34.5	33.1	CABG x 3 • LIMA → LAD • RIMA → Ramus (w/ endarterectomy) • Radial → PDA
CAD4 (48y/M)	Complex Multivessel • 100% mid-LAD • 100% mid-RCA • 99% LCx (Anomalous Org.)	50.0	49.9	CABG x 3 • LIMA → LAD • Radial → RCA/PL • SVG → Diagonal
CAD6 (72y/M)	Multivessel Disease • 50% LMCA, 70% proximal LAD • 90% OM2 • 95% mid-RCA	53.3	62.8	CABG x 3 • LIMA → LAD • SVG → OM • SVG → PDA

SUPPLEMENTARY TABLE 2. Patient Characteristics, Surgical Revascularization Details, and Left Ventricular Ejection Fraction. This table summarizes the preoperative coronary anatomy, surgical grafting strategies, and pre- and post-CABG left ventricular ejection fraction (LVEF) for five patients undergoing coronary artery bypass grafting (CABG). Information includes specific graft targets and LVEF values. Left ventricular ejection fraction (LVEF) values presented were derived from magnetic resonance (MR) volumetric analysis. Abbreviations: CABG, Coronary Artery Bypass Grafting; CAD, Coronary Artery Disease; LAD, Left Anterior Descending Artery; LCx, Left Circumflex Artery; LIMA, Left Internal Mammary Artery; LMCA, Left Main Coronary Artery; LVEF, Left Ventricular Ejection Fraction; OM, Obtuse Marginal Artery; PDA, Posterior Descending Artery; PL, Posterolateral; RCA, Right Coronary Artery; RIMA, Right Internal Mammary Artery; SVG, Saphenous Vein Graft.



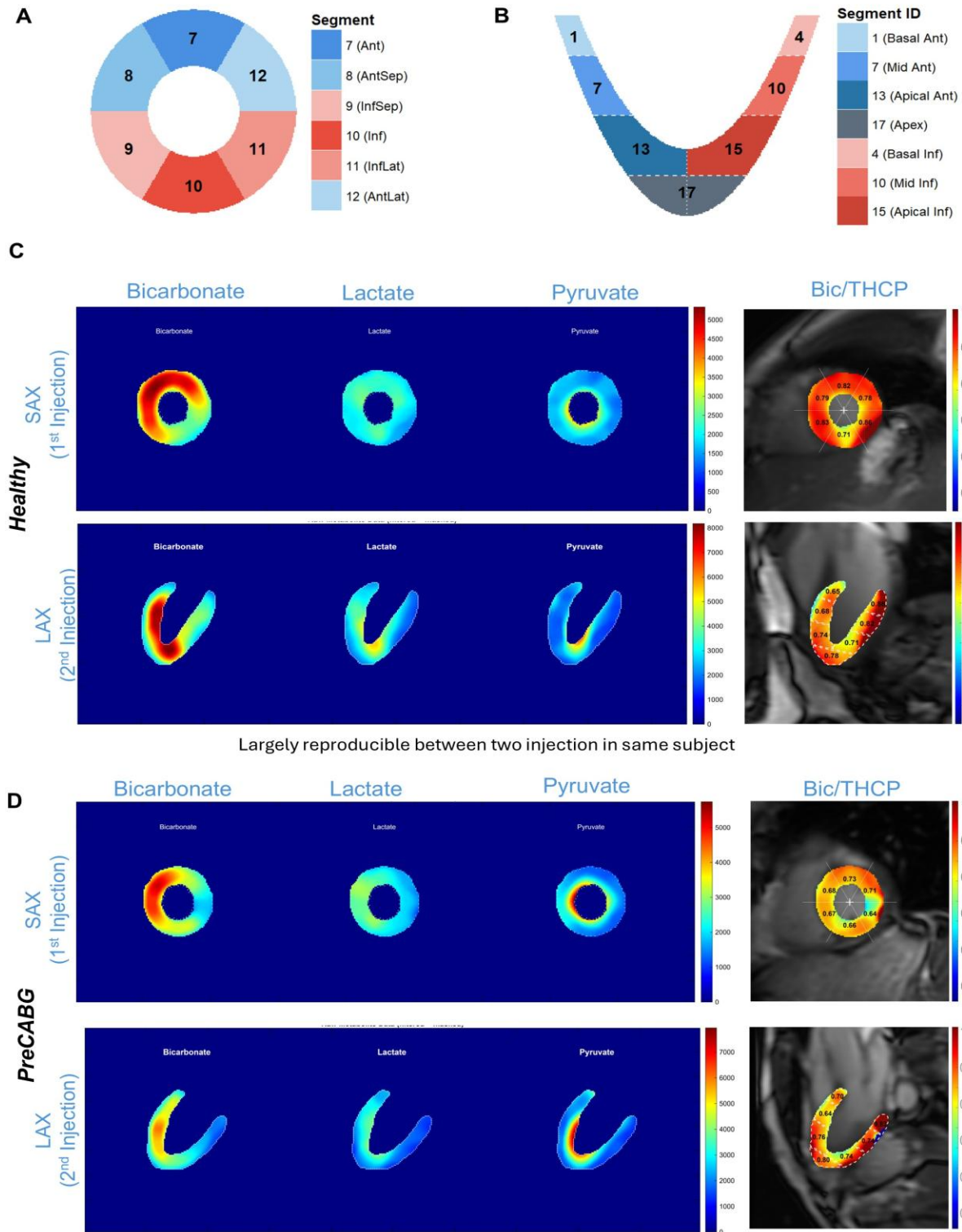
SUPPLEMENTARY FIGURE 1. Study Workflow and Quality Control Process: Comprehensive study workflow demonstrating the sequential steps from subject preparation through data analysis. The workflow includes: (1) Imaging probe preparation and fluid path assembly; (2) Clinical-grade polarization using the SPINlab system with multiprobe quality control (MPQC); (3) Anatomical reference imaging using ^1H cine MRI; (4) Hyperpolarized ^{13}C metabolic imaging; and (5) Data analysis including quantitation using HP- ^{13}C MRAnalyst and clinical correlation using Medis Suite. Subject monitoring included pre-examination blood draw and ECG, post-examination monitoring and ECG, questionnaire administration, physician review for discharge, and telephonic follow-up. MRI = magnetic resonance imaging; QC = quality control; RN = registered nurse.



C *HP¹³CMR-Analyst GUI*

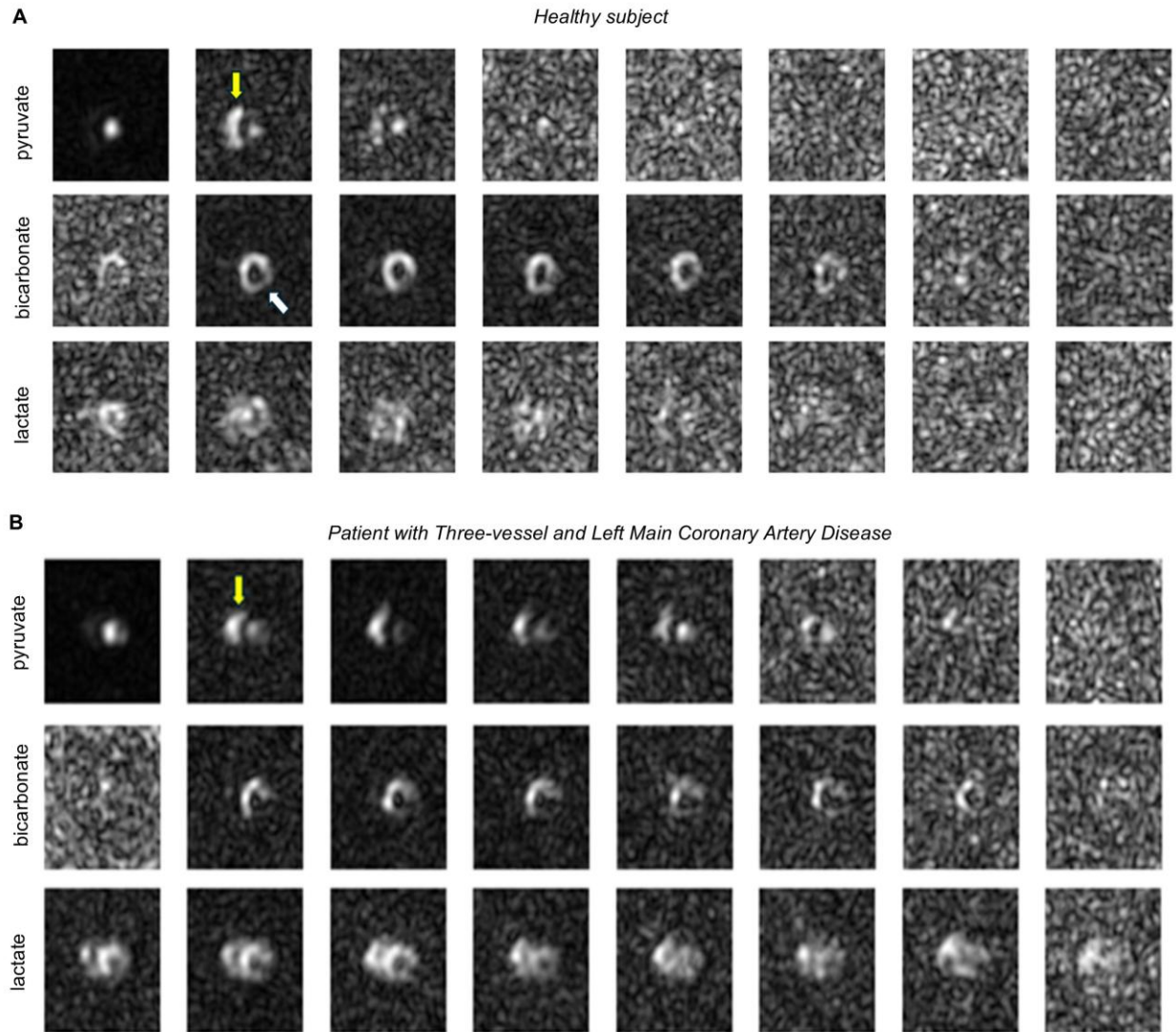
The screenshot shows the HP13CMR-Analyst GUI interface. At the top, there are tabs for 'Data Path', 'Visualization', 'Segmentation', 'Quantification', 'Kinetic Model', and 'Help'. Below these are buttons for 'SA Segment' and 'LA Segment'. A 'Folder content' list on the left includes files like '3CH_Cine_19', 'C13_MEspiral_LA_22_Metab1-3', 'C13_MEspiral_SA_14_Metab1-3', 'HLA_Cine_(Long_BH_PW)_7', 'Matlab_matrix', and 'SA Cine MS 20'. A '2.DCM2MAT Convert' section contains input fields for 'SA_Bic', 'SA_Lac', 'SA_Pyr', 'LA_Bic', 'LA_Lac', 'LA_Pyr', and 'SA_Cine', all pointing to a directory path. On the right, 'Background-Subtracted Metabolite Maps' are displayed for Bicarbonate, Lactate, and Pyruvate, with a color scale from 0 to 3500. A 'Logs' window at the bottom shows the output saved to a specific file path.

SUPPLEMENTARY FIGURE 2. Myocardial Metabolism and HP-¹³CMRAnalyst Software Interface: (A) Metabolism of hyperpolarized pyruvate of healthy myocardium and ischemic myocardium. (B) Software interface displaying segmental analysis tools and metabolic ratio calculations. Representative analysis of ischemic myocardium demonstrating reduced bicarbonate signal in affected territories. The software enables automated segmentation according to the American Heart Association 17-segment model, time-resolved signal extraction, and kinetic parameter estimation using the input-less fitting method.

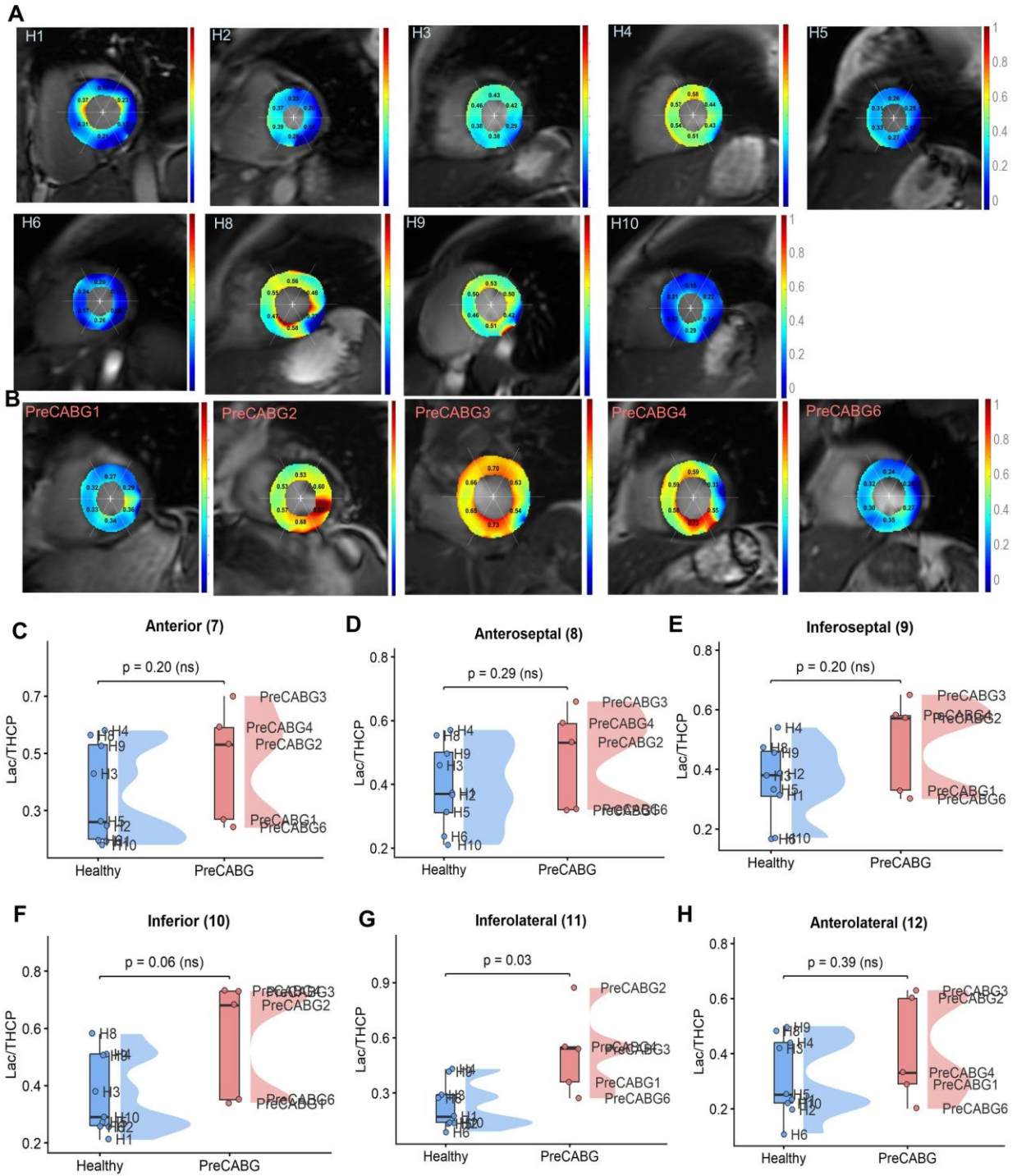


SUPPLEMENTARY FIGURE 3. Reproducibility Assessment: (A-B) American Heart Association 17-segment model reference diagrams. **(C)** Healthy subject imaging views of along short-axis (SAX) and long-axis (LAX) demonstrating metabolite maps and Bic/THCP overlays on

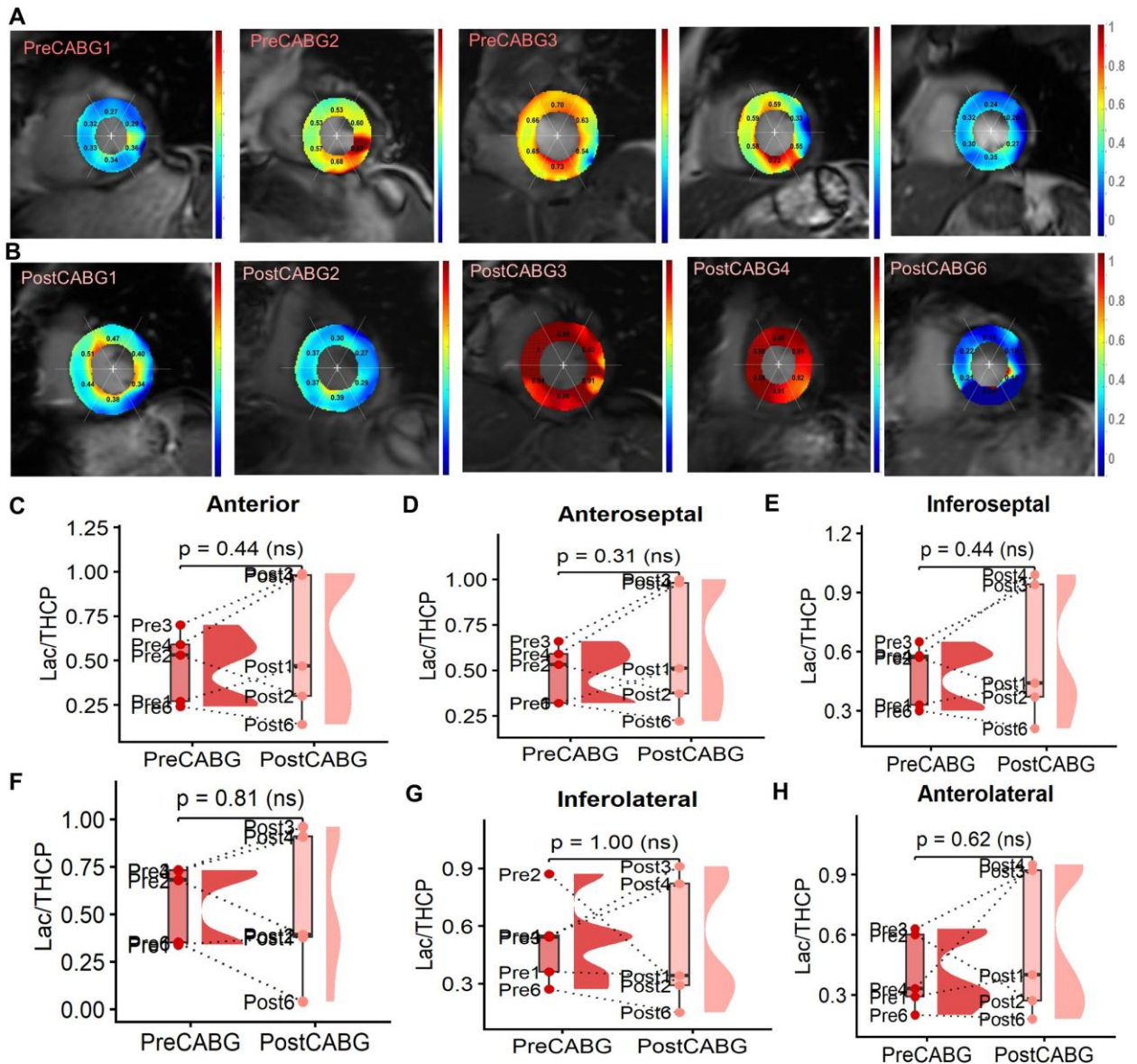
anatomic image from same imaging session. **(D)** Pre-CABG patient different imaging views of along SAX and LAX metabolite maps and Bic/THCP overlays on anatomic image from same imaging session. Reproducibility between injections supports the reliability of the metabolic quantification approach.



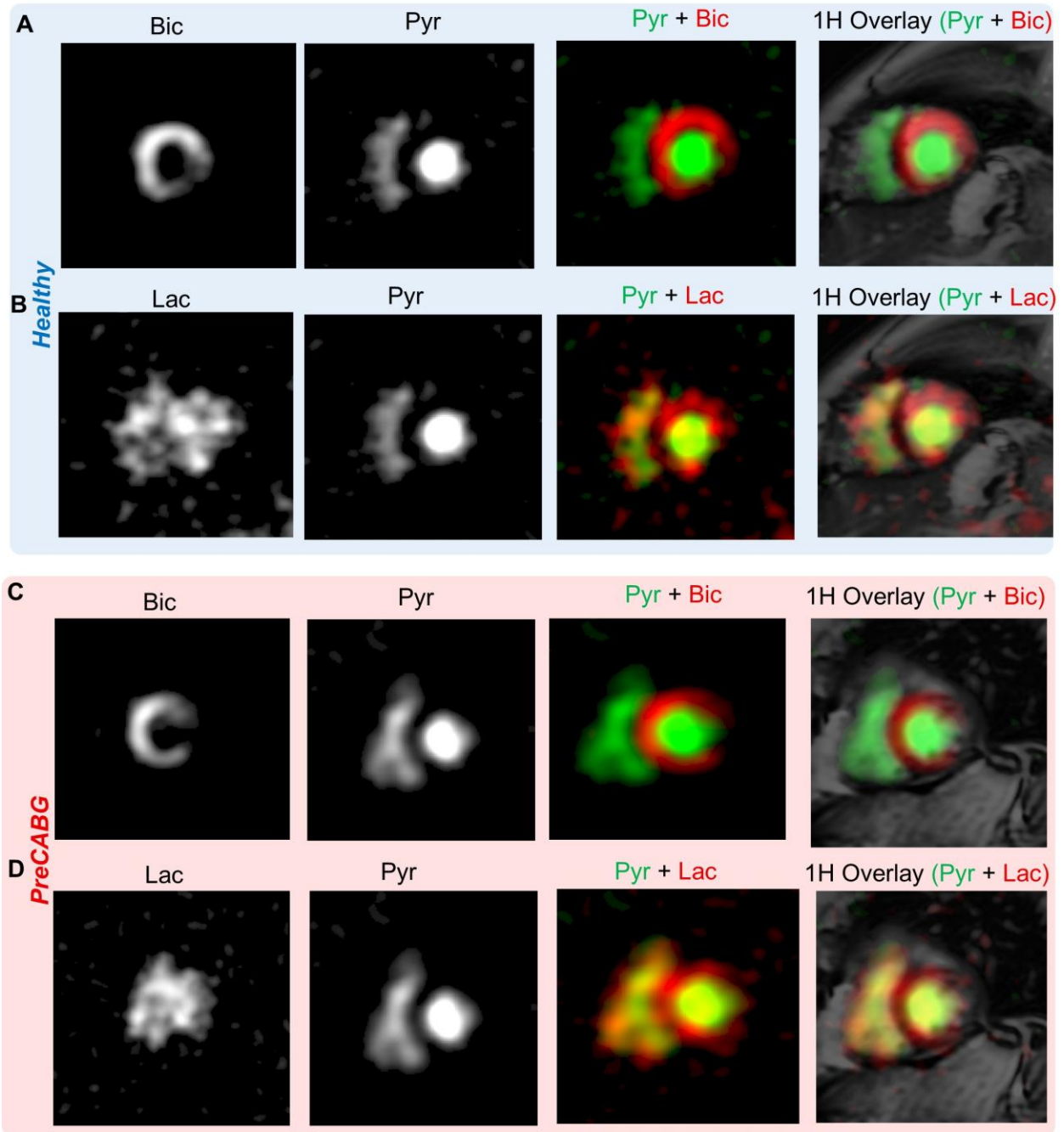
SUPPLEMENTARY FIGURE 4. Myocardial Pyruvate Metabolism in Healthy versus Three-Vessel Coronary Artery Disease. (A) Healthy Control Subject: Sequential images acquired at one frame per heartbeat, beginning 25 seconds post-injection. The upper row demonstrates [^{13}C]pyruvate in the left ventricular cavity, with right ventricular recirculation indicated by the yellow arrow. Normal oxidative conversion to [^{13}C]bicarbonate (middle row, with segment 11 marked by a white arrow) and reduction to [^{13}C]lactate (bottom row) are clearly visualized. **(B) Coronary Artery Disease Patient:** Corresponding images from a patient with three-vessel and left main disease. Compared to the healthy control, the ischemic myocardium exhibits a distinct temporal delay in the appearance of the [^{13}C]bicarbonate signal.



SUPPLEMENTARY FIGURE 5. Lactate/THCP Ratio Maps: **(A)** Lac/THCP ratio maps for all healthy controls (H1-H10, excluding H7). **(B)** Lac/THCP ratio maps for pre-CABG patients (PreCABG1-PreCABG6, excluding PreCABG5) showing regional heterogeneity with trends toward higher lactate production in ischemic territories, reflecting increased reliance on anaerobic glycolysis. **(C-H)** Quantitative comparison by segment between healthy controls and pre-CABG patients. Reciprocal to Bic/THCP ratios in ischemic territories, increased Lac/THCP with statistical significance ($p=0.03$) in segment 11 in this cohort. Lac = lactate; THCP = total hyperpolarized carbon-13 product.

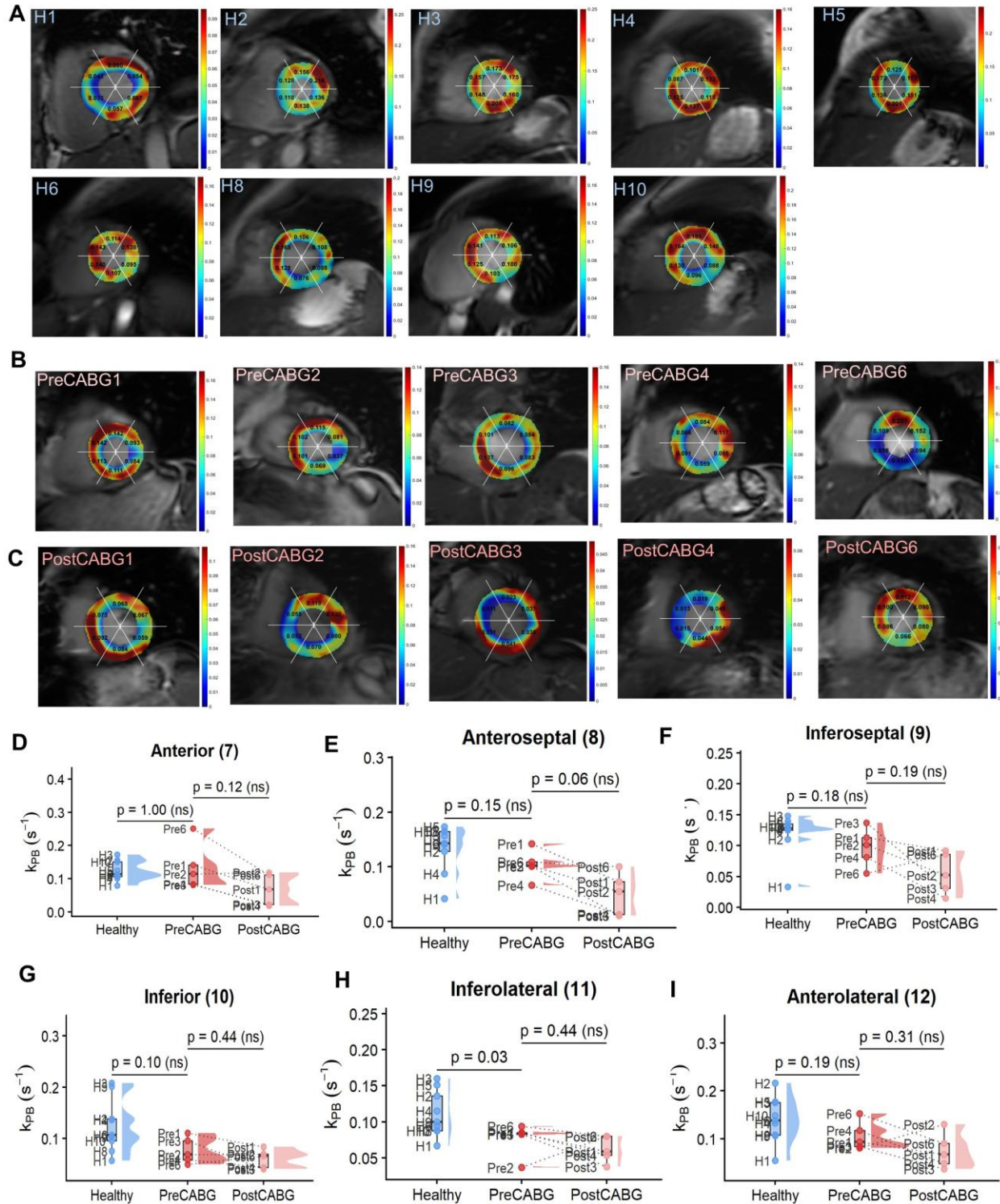


SUPPLEMENTARY FIGURE 6. Pre-CABG vs Post-CABG Lactate/THCP Comparison: (A) Lactate/THCP ratio maps for pre-CABG patients. **(B)** Corresponding post-CABG maps for the same patients. **(C-H)** Quantitative regional comparison of Lactate/THCP ratios. Heterogenous lactate production trends observed in ischemic territories following surgical revascularization.



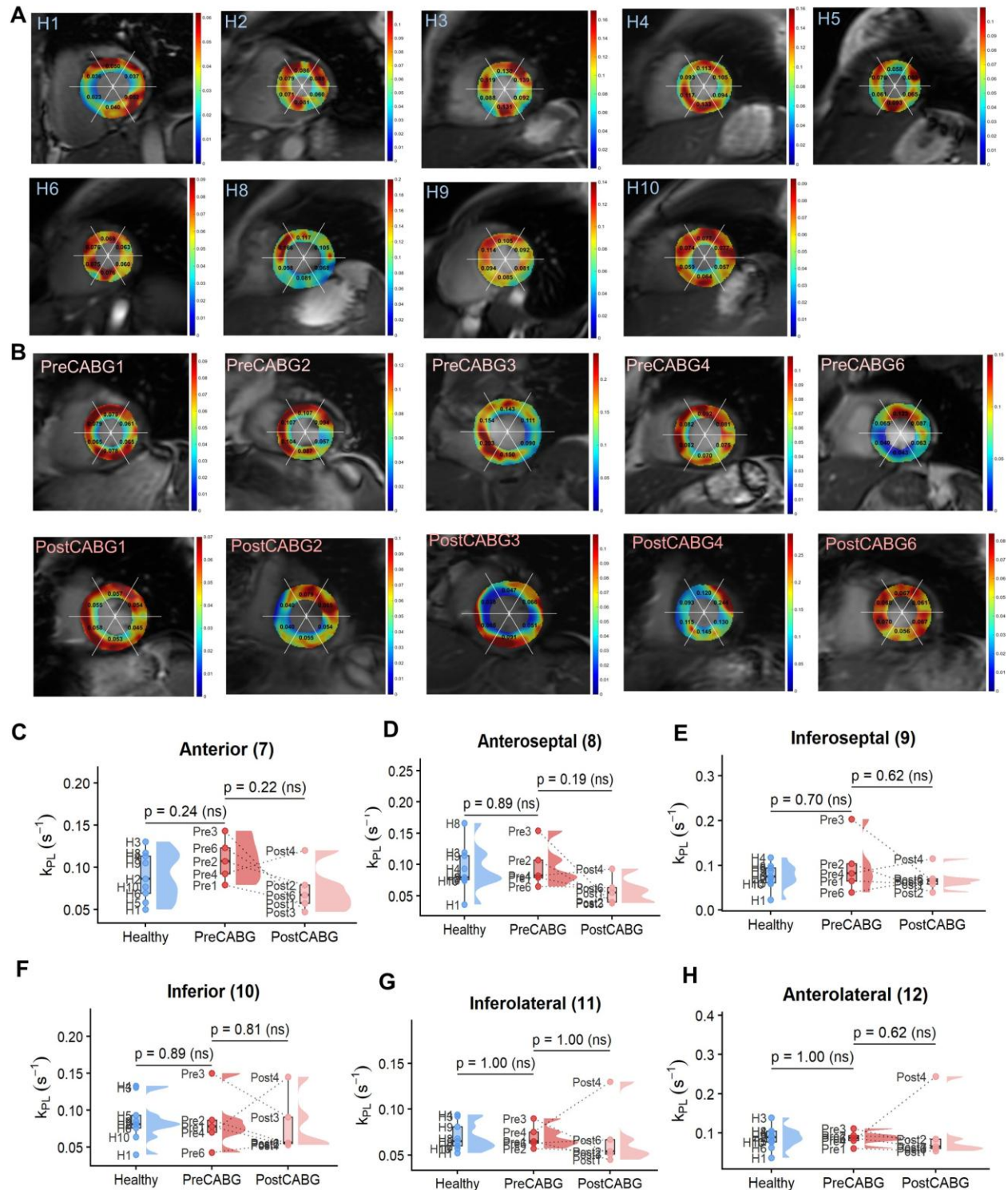
SUPPLEMENTARY FIGURE 7. Anatomical Overlay of Metabolite Maps: (A-B) Representative healthy subject showing individual metabolite maps (Bic, Lac, Pyr) and combined overlays on ^1H anatomical images. Pyruvate plus bicarbonate (Pyr+Bic) and pyruvate plus lactate (Pyr+Lac) overlays demonstrate cardiac localization and metabolite distribution. **(C-D)** Representative pre-CABG patient showing corresponding metabolite maps and anatomical overlays. Note the regional differences in Bic signal between healthy and ischemic myocardium. These overlays

confirm accurate cardiac localization of the hyperpolarized ^{13}C signal and enable correlation with anatomical structures. Bic = bicarbonate; CABG = coronary artery bypass grafting; Lac = lactate; Pyr = pyruvate.



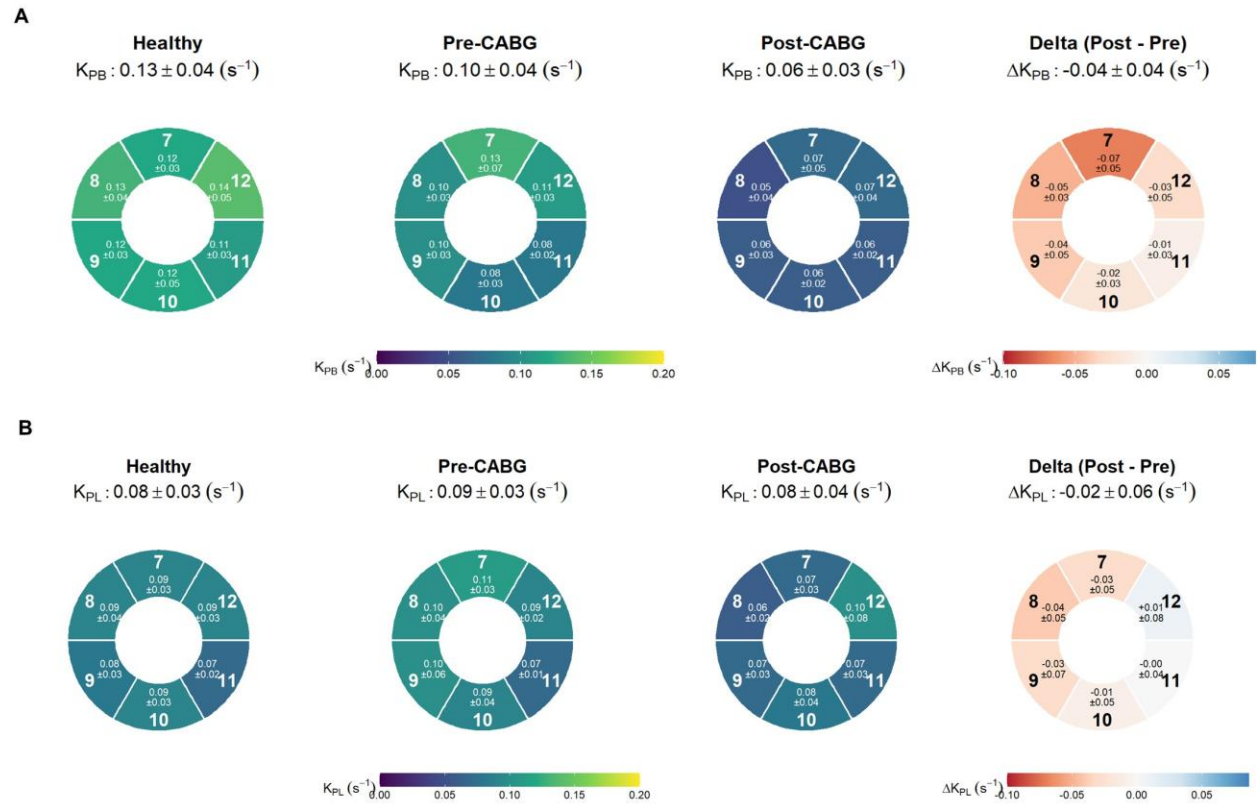
SUPPLEMENTARY FIGURE 8. k_{PB} Rate Constant Maps (A) Rate constant maps (k_{PB}) for healthy controls. (B) k_{PB} Maps for pre-CABG patients. (C) Corresponding post-CABG maps. (D-I) Quantitative regional comparison of kinetic parameters showing trends following CABG. CABG

= coronary artery bypass grafting; k_{PB} = apparent rate constant for pyruvate-to-bicarbonate conversion.



SUPPLEMENTARY FIGURE 9. k_{PL} Rate Constant Maps (A) k_{PL} (pyruvate-to-lactate rate constant) maps for all healthy controls (H1-H10, excluding H7). (B-E) k_{PL} maps for pre-CABG patients. (F-H) Corresponding post-CABG k_{PL} maps for the same patients. k_{PL} values remained

relatively stable following CABG, consistent with the interpretation that metabolic recovery primarily involves enhanced oxidative (k_{PB}) rather than altered glycolytic (k_{PL}) activity. The combination of k_{PL} and k_{PB} provides complementary information about pyruvate fate and metabolic flexibility. CABG = coronary artery bypass grafting; k_{PL} = apparent rate constant for pyruvate-to-lactate conversion.



SUPPLEMENTARY FIGURE 10. Regional Apparent Rate Constant Polar Maps for Pyruvate Conversion. (A) K_{PB} Polar Maps: Segmental distribution of the apparent pyruvate to bicarbonate conversion rate (K_{PB}) across healthy controls, pre-CABG patients, and post-CABG patients, including a quantitative delta map highlighting postoperative changes. (B) K_{PL} Polar Maps: Corresponding segmental distribution of the apparent pyruvate to lactate conversion rate (K_{PL}). These visualizations demonstrate the relative stability of K_{PL} alongside the dynamic shifts in K_{PB} following surgical revascularization.

SUPPLEMENTARY METHODS

Enrollment Criteria

A thorough pre-enrollment assessment was conducted, involving comprehensive medical history collection and systematic review of existing patient records. Potential participants were carefully selected based on strict inclusion and exclusion parameters designed to ensure a homogeneous study population. All subjects were sedentary adults, representing the primary demographic of interest. Control subjects were specifically excluded if they had significant underlying medical conditions, including untreated or complex cardiovascular disease (with only mild hypertension managed by single-agent therapy permitted), hepatic disorders such as cirrhosis or chronic hepatitis, endocrine abnormalities like diabetes or thyroid dysfunction, known malignancies, or other serious systemic illnesses. Additional exclusions included standard MRI contraindications such as metal implants or claustrophobic limitations, as well as positive pregnancy test results for women with reproductive potential. Trained study personnel from the Clinical Trials Office from the Cardiovascular and Thoracic Surgery completed detailed consent discussions and screening protocols on the day of enrollment, ensuring all participants met the precise research criteria and understood the study's requirements.

Postoperative Metabolic Changes and Clinical Course of CAD subjects

Changes in metabolic parameters before and after CABG were heterogeneous and somewhat inconsistent (Supplementary Table 2). However, closer review of the clinical course of the patients undergoing coronary revascularization provides some insights. Two of the patients suffered perioperative myocardial infarctions (STEMI in CAD3 with subsequent LAD PCI) and NSTEMI in CAD4 (whose circumflex territory was ungraftable). In both patients, post-operative Bic/THCP ratios were lower in the post-CABG studies. Patient CAD2 underwent uncomplicated revascularization and showed higher postoperative Bic/THCP. Patient CAD6 developed a new right bundle branch block (RBBB) after surgery and echocardiographic evidence of a new inferior wall motion abnormality. The postoperative study showed a decrease in the ratio in segment 10 corresponding to the LV inferior wall. While more study is required, these data may

suggest a relationship between success in coronary revascularization and subsequent myocardial oxidative metabolism.

Kinetic Analysis Protocol

Theoretical Framework

While this study was not primarily designed to determine kinetic rate constants, we explored the feasibility of such calculations. Kinetic analysis of hyperpolarized [1-¹³C]pyruvate data employed a unidirectional two-site exchange model describing the conversion of pyruvate to metabolic products (lactate, bicarbonate). This model assumes that the forward reactions catalyzed by lactate dehydrogenase (pyruvate to lactate) and pyruvate dehydrogenase (pyruvate to bicarbonate) dominate over back-exchange under the experimental conditions employed. This model describes the observable conversion of pyruvate to metabolic products (lactate, bicarbonate) during the acquisition window. Metabolic conversion occurring prior to image acquisition onset (~25 seconds post-injection) is not captured, and the estimated rate constants are therefore apparent values reflecting the observable kinetic window.

Differential Equations

The system was governed by the following coupled differential equations:

$$\text{For pyruvate: } dMPyr/dt = -R1P * MPyr - kPL * MPyr - kPB * MPyr + u(t)$$

$$\text{For lactate: } dMLac/dt = kPL * MPyr - R1L * MLac$$

$$\text{For bicarbonate: } dMBic/dt = kPB * MPyr - R1B * MBic$$

where M_{Pyr} , M_{Lac} , and M_{Bic} represent the longitudinal magnetization of pyruvate, lactate, and bicarbonate, respectively; k_{PL} and k_{PB} denote the apparent rate constants for pyruvate-to-lactate and pyruvate-to-bicarbonate conversion (s^{-1}); $R1P$, $R1L$, and $R1B$ represent the longitudinal relaxation rates ($= 1/T1$) for each metabolite (s^{-1}); and $u(t)$ represents the input function describing pyruvate delivery.

Input-less Fitting Method

The analysis employed an input-less method that eliminates the need to model the arterial input function, which is advantageous in clinical settings where bolus kinetics may be variable. This approach uses the measured pyruvate signal directly as the driving function for product generation. The input $u(t)$ was estimated from the pyruvate signal at each time point according to:

$$u(t) = [MPyr(t + 1) - MPyr(t) * \exp(-(R1P + kPL + kPB) * TR)] / [1 - \exp(-(R1P + kPL + kPB) * TR)] * (R1P + kPL + kPB)$$

Signal Normalization

Before kinetic fitting, signals were normalized to the 99th percentile of the pyruvate signal according to: $S_{norm}(t) = S(t) / P99(S_{Pyr})$. This normalization reduces inter-subject variability arising from differences in polarization levels, injection efficiency, and cardiac output, enabling meaningful comparison of kinetic rate constants across subjects and time points.

RF Flip Angle Correction

The observed transverse magnetization (M_{xy}) was converted to longitudinal magnetization (M_z) accounting for the metabolite-specific flip angles: $M_z(t) = M_{xy}(t) / \sin(\theta)$, where theta (θ) represents the flip angle for each metabolite at each time point (pyruvate 10 degrees, lactate 90 degrees, bicarbonate 90 degrees).

Default Parameter Values

The following default parameters were employed for kinetic fitting:

Repetition time (TR): Subject-specific R-R interval (average ~1.0 s)

Pyruvate flip angle (θ_{Pyr}): 10°

Lactate flip angle (θ_{Lac}): 90°

Bicarbonate flip angle (θ_{Bic}): 90°

Pyruvate R1 (R1P): 0.04 s⁻¹ (fixed, corresponding to T1 = 25 s)

Initial k_{PL} estimate: 0.02 s⁻¹

Initial R1L estimate: 0.04 s⁻¹

Fixed vs. Fitted Parameters

R1P was fixed at 0.04 s^{-1} based on prior validation studies demonstrating that pyruvate T1 is well-characterized and fixing this parameter improves fit stability. k_{PL} , k_{PB} , and $R1L$ were fitted as free parameters. k_{PL} and k_{PB} represent the primary parameters of interest reflecting metabolic conversion. R1L was fitted because lactate T1 may vary with the tissue environment.

Optimization Algorithm

Parameter estimation employed nonlinear least-squares fitting using the Levenberg-Marquardt algorithm. The objective function minimized the sum of squared residuals between measured and model-predicted metabolite signals across all time points. Fitting was performed independently for each myocardial segment according to the American Heart Association 17-segment model. Convergence criteria included parameter change tolerance of 10^{-6} and function tolerance of 10^{-6} . Initial parameter estimates were updated iteratively until convergence or maximum iteration count (1000) was reached.

Quality Control and Exclusion Criteria

Fitted parameters were subject to quality control assessment. Segments were excluded from analysis if: peak pyruvate signal-to-noise ratio was less than 10; fitting failed to converge; estimated k_{PL} or k_{PB} exceeded physiologically plausible bounds (greater than 0.2 s^{-1}); or coefficient of variation of fitted parameters exceeded 50%. These criteria ensured that reported metabolic parameters reflect reliable estimates.